

LINE-OF-SIGHT STRUCTURE TOWARD STRONG LENSING GALAXY CLUSTERS*

MATTHEW B. BAYLISS^{1,2}, TRACI JOHNSON³, MICHAEL D. GLADDERS^{4,5}, KEREN SHARON³ AND MASAMUNE OGURI^{6,7}
Draft version September 5, 2021

ABSTRACT

We present an analysis of the line-of-sight structure toward a sample of ten strong lensing cluster cores. Structure is traced by groups that are identified spectroscopically in the redshift range, $0.1 \leq z \leq 0.9$, and we measure the projected angular and comoving separations between each group and the primary strong lensing clusters in each corresponding line of sight. From these data we measure the distribution of projected angular separations between the primary strong lensing clusters and uncorrelated large scale structure as traced by groups. We then compare the observed distribution of angular separations for our strong lensing selected lines of sight against the distribution of groups that is predicted for clusters lying along random lines of sight. There is clear evidence for an excess of structure along the line of sight at small angular separations ($\theta \leq 6'$) along the strong lensing selected lines of sight, indicating that uncorrelated structure is a significant systematic that contributes to producing galaxy clusters with large cross sections for strong lensing. The prevalence of line-of-sight structure is one of several biases in strong lensing clusters that can potentially be folded into cosmological measurements using galaxy cluster samples. These results also have implications for current and future studies – such as the Hubble Space Telescope Frontier Fields – that make use of massive galaxy cluster lenses as precision cosmological telescopes; it is essential that the contribution of line-of-sight structure be carefully accounted for in the strong lens modeling of the cluster lenses.

Subject headings: galaxies: clusters: strong lensing — galaxies: distances and redshifts — techniques: spectroscopic — large-scale structure of universe

1. INTRODUCTION

Strong lensing galaxy clusters are a small and extreme subset of the general cluster population, and as such, cluster lenses provide a valuable tracer of the rarest and most over-dense regions in the cosmic web. The abundance of galaxy cluster-scale strong lenses can be compared against predictions of the global strong lensing efficiency of galaxy clusters in simulations to test the concordance cosmological paradigm. The typical measurement that is made is the number density of giant arcs that are observed around samples of massive galaxy clusters (“giant arc statistics”, see

the review by Meneghetti et al. 2013). Because cluster-scale lenses are rare these comparisons have historically been limited to using very small observational samples of arcs, but the results consistently find a significant excess of arcs observed compared to predictions from simulations (Grossman & Narayan 1988; Bartelmann et al. 1998; Cooray 1999; Luppino et al. 1999; Zaritsky & Gonzalez 2003; Gladders et al. 2003; Li et al. 2006; Hennawi et al. 2007; Horesh et al. 2011; Meneghetti et al. 2011). The notable difference between the frequency of giant arcs forming around massive clusters has been labeled the “giant arc statistics problem” for more than a decade (Bartelmann et al. 1998).

Reconciling the difference between the abundance of giant arcs predicted and observed is an outstanding problem in observational cosmology, and solving this problem requires an improved understanding of the detailed astrophysics that contribute to the global strong lensing properties of massive clusters. The physical processes that are responsible for making a small fraction of massive clusters into efficient gravitational lenses are not fully understood. Understanding these processes is also important because galaxy cluster strong lenses provides us with the best “natural telescopes” for studying the distant universe, and several large observational initiatives are underway (CLASH; Postman et al. 2012) or planned (e.g., the Hubble Space Telescope Frontier Fields⁹) that will rely on using precision strong lens modeling of the magnification by strong lensing galaxy clusters to study the background universe.

A variety of different astrophysical effects can be invoked to explain how cluster lenses come to have large strong lensing cross sections, and to alleviate the

mbayliss@cfa.harvard.edu

* From observations taken with the MMT Observatory, a joint facility of the Smithsonian Institution and the University of Arizona; the 6.5 meter Magellan Telescopes located at Las Campanas Observatory, Chile; with the Gemini Observatory, which is operated by the Association of Universities for Research in Astronomy, Inc., under a cooperative agreement with the NSF on behalf of the Gemini partnership: The United States, Canada, Chile, Australia, Brazil and Argentina; and with the Subaru Telescope, which is operated by the National Astronomical Observatory of Japan

¹ Department of Physics, Harvard University, 17 Oxford St., Cambridge, MA 02138

² Harvard-Smithsonian Center for Astrophysics, 60 Garden St., Cambridge, MA 02138

³ Department of Astronomy, the University of Michigan, 500 Church St. Ann Arbor, MI 48109

⁴ Department of Astronomy & Astrophysics, University of Chicago, 5640 South Ellis Avenue, Chicago, IL 60637

⁵ Kavli Institute for Cosmological Physics, University of Chicago, 5640 South Ellis Avenue, Chicago, IL 60637

⁶ Department of Physics, University of Tokyo, Tokyo 113-0033, Japan

⁷ Kavli Institute for the Physics and Mathematics of the Universe (Kavli IPMU, WPI), University of Tokyo, Chiba 277-8583, Japan

⁹ <http://www.stsci.edu/hst/campaigns/frontier-fields/>

TABLE 1
SPECTROSCOPIC OBSERVATIONS

Cluster Name	α (J2000.0)	δ (J2000.0)	UT Date	Instrument	Disperser	Filter
Abell 1703	13 15 05.24	+51 49 02.6	Mar 17 2012	MMT/Hectospec	270 1/mm Grating	–
SDSS J0851+3331	08 51 38.86	+33 31 06.1	Feb 19 2012	MMT/Hectospec	270 1/mm Grating	–
SDSS J0915+3826	09 15 39.00	+38 26 58.5	Feb 19 2012	MMT/Hectospec	270 1/mm Grating	–
SDSS J0957+0509	09 57 38.50	+05 09 21.6	Jan 27 2009	Magellan/IMACS+GISMO	150 1/mm Grating	WB4800-7800
SDSS J0957+0509	09 57 37.34	+05 09 49.9	Apr 09 2013	Magellan/IMACS f/2	200 1/mm Grism	–
SDSS J1038+4849	10 38 42.90	+48 49 18.7	Mar 16 2012	MMT/Hectospec	270 1/mm Grating	–
SDSS J1050+0017 ^a	10 50 40.20	+00 16 17.6	Mar 17 2013	Magellan/IMACS f/2	200 1/mm Grism	–
SDSS J1050+0017 ^a	10 50 40.20	+00 16 17.6	Mar 17 2013	Magellan/IMACS f/2	200 1/mm Grism	–
SDSS J1050+0017	10 50 41.83	+00 17 18.1	Mar 29 2012	Gemini/GMOS North	R400 Grating	OG515
SDSS J1152+3313	11 52 00.15	+33 13 42.1	Mar 16 2012	MMT/Hectospec	270 1/mm Grating	–
SDSS J1226+2149	12 26 51.11	+21 49 52.3	Feb 19 2012	MMT/Hectospec	270 1/mm Grating	–
SDSS J1226+2149 ^b	12 26 50.70	+21 52 38.4	Apr 20 2009	Magellan/IMACS+GISMO	150 1/mm Grating	WB4800-7800
SDSS J1226+2149	12 26 50.42	+21 49 53.0	Apr 21 2009	Magellan/IMACS+GISMO	150 1/mm Grating	WB4800-7800
SDSS J1226+2149 ^b	12 26 50.70	+21 52 38.4	May 27 2009	Magellan/IMACS+GISMO	300 1/mm Grating	WB4300-6750
SDSS J1329+2243	13 29 36.54	+22 43 16.7	Jun 02 2011	Gemini/GMOS North	R400 Grating	OG515
SDSS J1329+2243	13 29 34.50	+22 43 16.2	Apr 09 2013	Magellan/IMACS f/2	200 1/mm Grism	WB3800-7000

^a SDSS J1050+0017 was observed with two different multi-slit masks on March 17, 2012.

^b One GISMO mask for SDSS J1226+2149 was re-observed in May 2009 due to poor weather during the exposures in Apr 2009.

tension between measurements of giant arc statistics and predictions from simulations. In addition to understanding line-of-sight structure, potentially important factors include accounting for baryons in the form of central massive galaxies and substructure (Flores et al. 2000; Meneghetti et al. 2003; Hennawi et al. 2007; Meneghetti et al. 2010), cooling baryons dragging dark matter into cluster cores (Puchwein et al. 2005; Rozo et al. 2008; Wambsganss et al. 2008; Blanchard et al. 2013), major mergers (Torri et al. 2004; Fedeli et al. 2006; Redlich et al. 2012), and the redshift distribution of the background galaxy source population (Hamana & Futamase 1997; Oguri et al. 2003; Wambsganss et al. 2004; Bayliss et al. 2011a; Bayliss 2012), and also more exotic cosmological explanations such as primordial non-gaussianity (D’Aloisio & Natarajan 2011b).

Each of the factors described above focuses on the properties in the lens or source planes, where the typical implicit assumption in the description of a strong lensing system is that the lensing potential of a strong lens is concentrated in a single region with a size that is much smaller than the distances separating the observer/lens/source – i.e., a single virialized structure such as a galaxy group or cluster. This simplifying assumption is convenient in that it confines the deflections due to gravitational lensing to a single plane, but neglects deflections due to other intervening mass distributions along the line of sight between the observer and the source. Furthermore, studies of simulated halos indicate that line-of-sight structure can introduce non-negligible systematic uncertainties in lensing-based measurements (Dalal et al. 2005; King & Corless 2007).

Ray tracing in simulations provides a range of results regarding the contribution of line-of-sight structure to galaxy cluster scale strong lenses (Wambsganss et al. 2005; Hilbert et al. 2007; Puchwein & Hilbert 2009; D’Aloisio & Natarajan 2011a; D’Aloisio et al. 2013), but observational constraints are so far nonexistent. There are individual examples in the literature of galaxy-scale lenses that receive boosts to their strong lensing cross sections due to intervening structure – typically galaxy groups and clusters along the line of sight

(Fassnacht et al. 2006; Wong et al. 2011), as well as studies of the statistical relationship between galaxy-scale lenses and large scale structure tracers such as galaxy environmental density (Faure et al. 2009; Fassnacht et al. 2011). These studies focus on smaller gravitational lenses (e.g., small Einstein radius, $r_E \lesssim 3.5''$); there is a notable lack of work exploring the importance of line-of-sight structure in real sample of galaxy cluster scale strong lenses, i.e., the most powerful gravitational lenses in the universe. In this paper we examine the line-of-sight structure toward a sample of galaxy clusters selected specifically for their strong lensing properties and high magnifications.

This paper is organized as follows: in § 2 we describe the origin and reduction of the spectroscopic data sets that inform our analyses. In § 3 we identify spectroscopic members of the primary lensing clusters, as well as over-densities in redshift space that indicate the presence of likely projected structures along the line of sight. In § 4 we discuss the constraints that our observations provide on the frequency with which uncorrelated structures contribute toward the strong lensing cross section of massive galaxy clusters, and in § 5 we summarize our results and their implications. All cosmological calculations performed for this paper assume a standard flat Λ cold dark matter (Λ CDM) cosmology with $H_0 = 73$ km s⁻¹ Mpc⁻¹, and matter density $\Omega_M = 0.25$. Magnitudes presented in this paper are in the AB system, calibrated against the SDSS.

2. CLUSTER SAMPLE AND OBSERVATIONS

2.1. The Sloan Giant Arcs Cluster Lens Sample

Incidents of strong lensing are identifiable by the formation of giant arcs, which are multiply imaged background sources that have been highly magnified by a foreground gravitational potential. The galaxy clusters studied in this work are drawn from the Sloan Giant Arcs Survey (SGAS; Gladders et al. in prep); numerous SGAS lenses, including the strong lensing systems studied here, have been previously published as used for various astrophysical and cosmological analyses (Oguri et al. 2009; Koester et al.

TABLE 2
EXAMPLE GALAXY REDSHIFT SAMPLE

Galaxy ID	α (J2000.0)	δ (J2000.0)	g mag	σ_g	r mag	σ_r	i mag	σ_i	redshift	$\sigma_{redshift}$
J131511.0+514653	13 15 11.07	+51 46 53.7	23.17	0.03	21.80	0.03	21.32	0.03	0.26900	0.00060
J131502.2+514951	13 15 02.26	+51 49 51.2	22.99	0.03	21.23	0.03	20.82	0.03	0.27070	0.00060
J131458.0+514916	13 14 58.10	+51 49 16.3	22.38	0.03	20.93	0.03	20.42	0.03	0.28860	0.00060
J131505.0+514606	13 15 05.04	+51 46 06.3	23.39	0.03	22.58	0.03	22.24	0.03	0.29090	0.00050
J131504.2+514750	13 15 04.26	+51 47 50.8	24.66	0.04	23.42	0.03	23.03	0.03	0.28000	0.00100
J131509.0+514622	13 15 09.01	+51 46 22.8	23.08	0.03	21.79	0.03	21.35	0.03	0.27050	0.00050
J131511.1+514557	13 15 11.12	+51 45 57.7	22.78	0.03	21.49	0.03	21.03	0.03	0.27660	0.00050
J131508.8+514545	13 15 08.89	+51 45 45.5	23.73	0.03	22.01	0.03	21.85	0.03	0.27810	0.00050
J131505.3+514536	13 15 05.37	+51 45 36.8	22.80	0.03	22.38	0.03	22.09	0.03	0.27660	0.00050
J131506.3+515428	13 15 06.39	+51 54 28.1	19.62	0.03	18.07	0.03	17.54	0.03	0.27400	0.00100

All magnitudes are AB.

2010; Bayliss et al. 2010, 2011a,b; Bayliss 2012; Oguri et al. 2012; Dahle et al. 2013; Gladders et al. 2013; Blanchard et al. 2013; Bayliss et al. 2013). We refer the reader to those papers, especially Bayliss et al. (2011b), for further information on the SGAS sample and how it was defined. The strong and weak lensing properties of the clusters analyzed here are all presented in detail in Oguri et al. (2012); the entire sample has Einstein radii $\theta_E > 5''$, and eight of the nine have $\theta_E \geq 9''$.

The subset of SGAS cluster lenses we focus on in this paper are those systems for which we have extensive spectroscopic followup (i.e., $\gtrsim 170$ redshifts) in the field centered on the primary galaxy cluster lens. In practice this selection stems from observations conducted in a pseudo-queue mode at the MMT observatory; the clusters discussed here were all part of a list of 25 SGAS clusters that were proposed for MMT/Hectospec observations. Unfortunately we were only able to observe six clusters with the MMT. The Hectospec data are supplemented by three clusters which were then observed from Magellan with IMACS (essentially those clusters far enough south to be observable from Las Campanas Observatory). The selection of the sample analyzed in this paper is independent of the known physical properties of the lenses (e.g., redshift, mass). All new spectroscopic observations presented in this paper are summarized in Table 1, and are supplemented by the available literature redshifts described in § 2.5.

2.2. MMT/Hectospec Spectroscopy

The majority of the spectroscopy presented in this paper was obtained using the Hectospec instrument (Fabricant et al. 2005) at the 6.5m MMT Observatory on Mt. Hopkins, AZ. Hectospec places 300 fibers over a region in the sky approximately 1 degree in diameter. In all fields observed with Hectospec fibers were placed on the sky using object selection and prioritization based on optical gri colors from deep Subaru/SuprimeCam imaging (Oguri et al. 2012). The total integration times for each field were 2-3 \times 1800 s. Hectospec data were reduced at the OIR Telescope Data Center and the Smithsonian Astrophysical Observatory using the pipeline of Mink et al. (2007), and redshifts measured using the RVSAO package (Kurtz & Mink 1998). Data were taken using the 270 line/mm grating, resulting in spectra with resolution, $R \sim 600-1500$ (200-500 km s $^{-1}$), covering a wavelength range $\Delta\lambda = 3650-9200$ angstroms. The RVSAO redshift uncertainties have been shown to be systematically

underestimated by a factor of ~ 2 (e.g., Quintana et al. 2000), so we use and report individual redshift measurements with uncertainties that are twice those that are output from RVSAO.

2.3. Magellan/IMACS Spectroscopy

Four clusters were observed with the Inamori-Magellan Areal Camera & Spectrograph (Dressler et al. 2006) on the 6.5m Magellan-I (Baade) telescope at Las Campanas Observatory. SDSS J1226+2153 was observed using the f/4 camera with the GISMO¹⁰ module; GISMO re-images the central $\sim 3.5'$ region within the IMACS field of view so as to enable a factor of $8\times$ spatial multiplexing of slit positions. A single GISMO mask places of order ~ 100 slits within this region of the sky, allowing for dense spectroscopic sampling. Two GISMO slit-masks were observed on Apr 20 & 21, 2009, one for 2×1800 s in clear conditions and one for 2×2400 s as clouds moved in. The second mask was re-observed in on May 27, 2009 due to the deteriorating cloud conditions limiting the quality of the data taken in Apr 2009; May observations were 3×1800 s. The two masks were each centered on one of the two strong lensing cores in SDSS J1226+2153. The masks were observed with the 150 line/mm grating and the WBP 4800-7800 order-blocking filter, resulting in spectral resolution $R \simeq 450-700$. The data were reduced using the COSMOS package¹¹, along with custom IDL code. Custom IDL routines were also used to extract the spectra and measure redshifts.

SDSS J1050+0017 was observed using IMACS with the f/2 camera on UT Mar 17 2013, and SDSS J0957+0509 and SDSS J1329+2243 were also observed with IMACS/f/2 on the UT Apr 09 2013. All of these observations used the 200 l/mm grism and the spectroscopic (i.e., no order blocking) filter and an unbinned detector, resulting in spectral resolution $R \simeq 500-1000$ (300-460 km s $^{-1}$) and sensitivity over the wavelength range $\Delta\lambda = 4800-9800\text{\AA}$. Two multi-slit masks were created for SDSS J1050+0017, and each mask was observed for 3×2400 s. A single mask was designed for each of SDSS J0957+0509 and SDSS J1329+2232, and these were exposed for 3×1500 s and 3×1800 s, respectively. The IMACS spectra for SDSS J1050+0017 are the same data used to inform strong lens modeling of that cluster lens in Bayliss et al. (2013).

¹⁰ www.lco.cl/telescopes-information/magellan/instruments/imacs/gismo/

¹¹ <http://code.obs.carnegiescience.edu/cosmos>

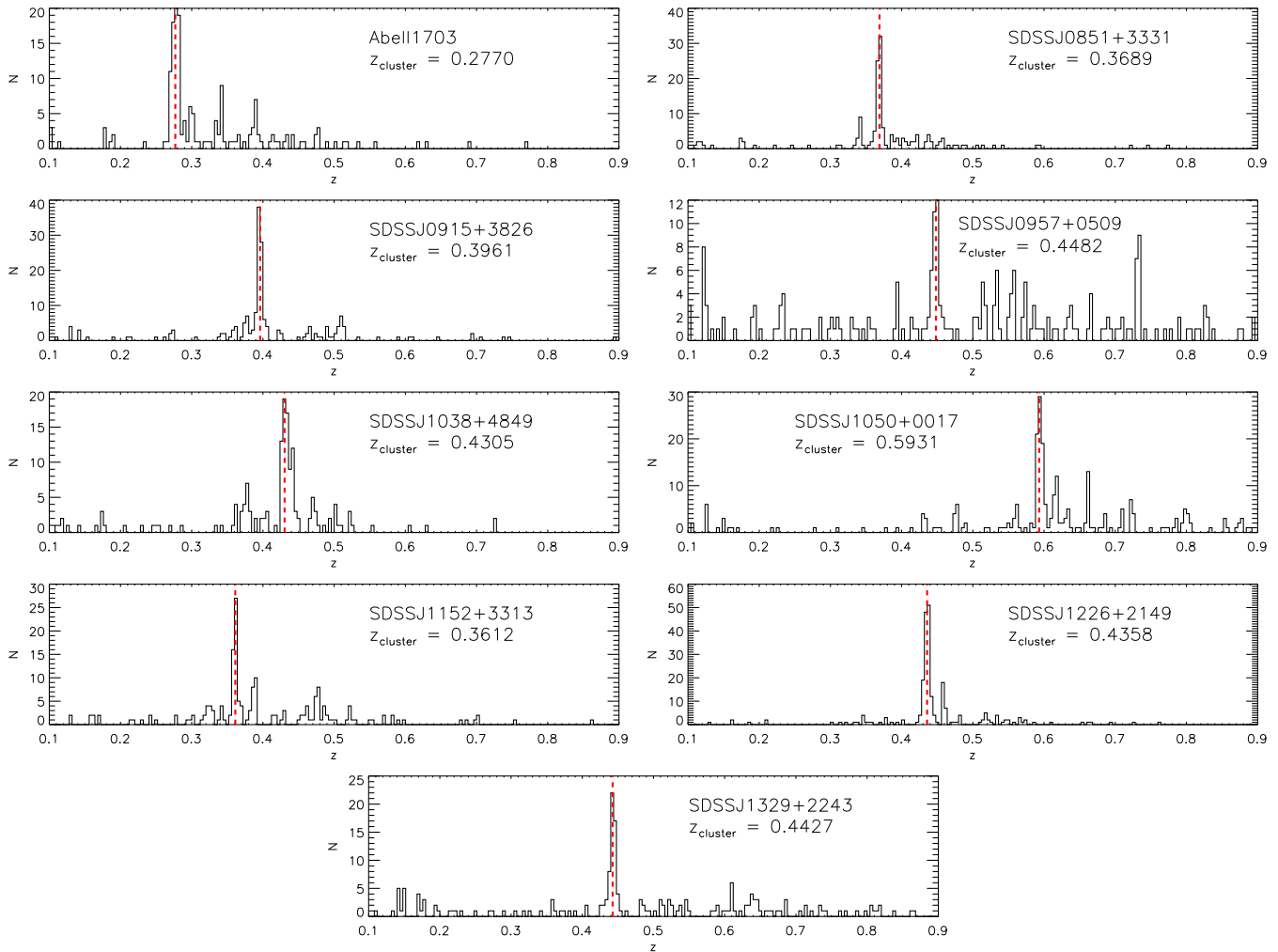


FIG. 1.— Redshift distributions for the fields centered on the strong lensing clusters analyzed here, sorted into recession velocity bins of width 1200 km s^{-1} . The bi-weight median redshift of each strong lensing cluster is indicated by a vertical red dashed line. Note that apparent overdensities in the velocity space plotted here do not necessarily correspond to physical structures due to the spatial distribution of the individual redshifts on the sky.

All masks were designed so as to place slits on a few faint, candidate strongly lensed background sources, with the remainder (and vast majority) of each mask devoted to placing slits on red-sequence selected cluster members and foreground/background field galaxies. All IMACS spectra were wavelength calibrated, bias subtracted, flat-fielded, and sky subtracted with the COSMOS reduction package, and then were extracted and stacked using custom IDL code.

2.4. Gemini/GMOS-North Spectroscopy

SDSS J1050+0017 and SDSS J1329+2243 also have previously unpublished redshift data from Gemini/GMOS-North that we include in our analysis. These data are almost identical to the spectra described in Bayliss et al. (2011b), with the exception that they were taken after the GMOS-North detectors were replaced with more sensitive e2vDD chips in November 2012. The primary goal of those observations was to obtain redshifts for lensed background sources, but open space in the mask was filled with red-sequence selected cluster members and other field galaxies.

The GMOS data were taken in macroscopic nod-and-

shuffle mode, so that sky subtraction simply requires differencing two regions of the detector. The data were wavelength calibrated, extracted, stacked, flux normalized, and analyzed with a custom pipeline that uses the XIDL¹² package. The resulting spectra cover a wavelength range $\Delta\lambda = 5600\text{-}10000\text{\AA}$, with a spectral resolution $R \simeq 700\text{-}1100$ ($270\text{-}430 \text{ km s}^{-1}$). The data reduction and redshift measurements were nearly identical to that used by Bayliss et al. (2011b), with the only changes being updates made to account for the new e2vDD detectors.

2.5. Supplemental Spectroscopy From the Literature

We supplement the new spectroscopic measurements described above with redshifts from Gemini+GMOS North published in Bayliss et al. (2011b), SDSS DR10 (Ahn et al. 2013) published redshifts, as well as redshifts for Abell 1703 published by Allen et al. (1992), Rizza et al. (2003), and Richard et al. (2009). In total our redshift completeness as a function of r -band magnitude is consistently $\sim 10\%$ down to $r_{AB} = 22$; this sparse

¹² <http://www.ucolick.org/~xavier/IDL/index.html>

sampling is not ideal, but still provides us with a rich dataset within which we can identify structures from the grouping of galaxies both in redshift and in spatial distribution on the sky.

Example galaxies from our full redshift catalog are shown in Table 2. The complete redshift catalogs used in this work have been made publicly available on the astronomy data repository on the Harvard Dataverse Network¹³.

3. REDSHIFT SAMPLE AND IDENTIFYING STRUCTURES

The redshift sample that we analyze here consists of all spectroscopic redshifts available from the data described in § 2 that fall within the field of view of the Suprime-Cam imager on the Subaru 8.2 m telescope (Suprime-Cam photometry/astrometry was used for target selection and slit/fiber placement for the vast majority of the observations described above). This results in a spectroscopic sample covering a region on the sky with dimensions $\sim 34' \times 27'$. We analyze nine such fields in this paper that cover a total solid angle of 2.3 deg^2 , containing ten unique strong lensing cluster cores.

3.1. Spectroscopic Cluster Members

There is an obvious spike in the redshift distribution for each of our fields at the redshift of the primary strong lensing cluster (Figure 1). We select cluster members from the spectroscopic catalog beginning with a by-eye guess of the cluster redshift – essentially the lens redshifts reported in Oguri et al. (2012) – and then compute an initial estimate using the bi-weight location and scale (Beers et al. 1990) of the velocity distribution for all redshifts within ± 0.02 in redshift, and within a projected physical radius, $R_{proj} \leq 1.5 \text{ Mpc}$. This projected radius corresponds approximately to the virial radius of these galaxy clusters. The choice of a physical cut in radius is somewhat arbitrary, but the resulting bi-weight median redshift estimates are insensitive to the exact choice. We then iteratively reject velocities separated from the bi-weight location by more than $\pm 3\sigma$ until convergence is reached. The total number of redshifts, number of spectroscopically confirmed cluster members (selected via the procedure described above), and bi-weight median redshifts of each primary cluster lens are presented in Table 3.

3.2. Identifying Line-of-Sight Structure

We identify additional structures by looking for over-densities in distribution of spectroscopically measured galaxies along the line of sight toward each cluster lens. We use a prescription based on the group catalog that was defined in the zCOSMOS 10k redshift survey (Knobel et al. 2009). Knobel et al. (2009) describe two methods for identifying group structures from redshift catalogs, and evaluate the performance of these methods using mock catalogs from simulations. Here we adopt the “Friends of Friends” (FoF) method, as it is the simpler of the two, having fewer free parameters than the alternative (VDM) algorithm, and the performance of the two methods is extremely similar.

TABLE 3
LINE-OF-SIGHT VELOCITY DATA

Cluster Name	N_z^a	N_c^b	$z_{cluster}$	σ_v (km s ⁻¹)
Abell1703	182	42	0.2770 ± 0.0010	1380 ± 140
SDSSJ0851+3331	169	41	0.3689 ± 0.0007	890 ± 130
SDSSJ0915+3826	218	39	0.3961 ± 0.0008	960 ± 120
SDSSJ0957+0509	280	25	0.4482 ± 0.0010	1250 ± 290
SDSSJ1038+4849	168	15	0.4305 ± 0.0008	550 ± 90
SDSSJ1050+0017	499	32	0.5931 ± 0.0005	560 ± 80
SDSSJ1152+3313	204	38	0.3612 ± 0.0007	800 ± 90
SDSSJ1226+2149 ^c	252	98	0.4358 ± 0.0004	870 ± 60
SDSSJ1329+2243	248	31	0.4427 ± 0.0007	830 ± 120

^a Size of the total spectroscopic galaxy sample in each field.

^b Number of cluster members within a projected physical radius of 1.5 Mpc.

^c This is a complex system that includes three different cluster-scale structures separated in recession velocity by a few hundred km s⁻¹; two of the three are strong lenses and separated by $\sim 2.5'$ on the sky.

The parameters of the FoF group finder are tuned to detect groups with different numbers of members (ie., $N \geq 6$, $N = 5$, $N = 4$, $N = 3$, and $N = 2$), based on extensive testing in mock catalogs (Knobel et al. 2009). We apply the FoF finder with these same optimized parameters (along with the galaxy number density computed from our own data) after removing the member galaxies of the primary strong lensing clusters— where member galaxies are defined from the criteria described in § 3.1. We characterize each group with a position on the sky equal to the mean right ascension and declination of the identified group members, and with a redshift computed using the bi-weight location estimator. From these quantities we measure the projected angular distance on the sky and the comoving distance along the line of sight (ie., perpendicular to the plane of the sky) between each strong lensing cluster core and the groups identified along their lines of sight. Example groups identified in our data are shown in Table 4. Where there are sufficient members to measure a dispersion ($N \geq 4$ using the gapper method; Beers et al. 1990) we find that the over-densities identified in our data have very small dispersions ($\sigma_v \lesssim 300 \text{ km s}^{-1}$; e.g., Table 4).

Structure in the universe is strongly correlated (e.g., Mo et al. 1996; Tadros et al. 1998), and the more massive the structure the stronger the correlation (Bahcall et al. 2003; Estrada et al. 2009). Structures that are separated by sufficiently small comoving radial distances are significantly more correlated than those with large comoving separations. Structure is, of course, correlated at a non-zero level out to extremely large scales (ie. hundreds of Mpc), but as a practical matter here we seek to identify “uncorrelated” structures as those structures that are not associated or interacting/merging with the primary lensing cluster. With a well-defined group sample in-hand, we now consider how to differentiate between groups that trace uncorrelated line-of-sight structure and groups that are located close enough to the primarily cluster lenses to be potentially interacting with them. It has also been shown that the mass distributions of massive clusters are aligned with surrounding filamentary structure, both in simulations (Noh & Cohn 2011) and in the SDSS (Smargon et al. 2012). These alignments are a manifestation of exactly the sort of correlated line of sight structure that we want to remove.

¹³ <http://thedata.harvard.edu/dvn/dataverses/cfa>

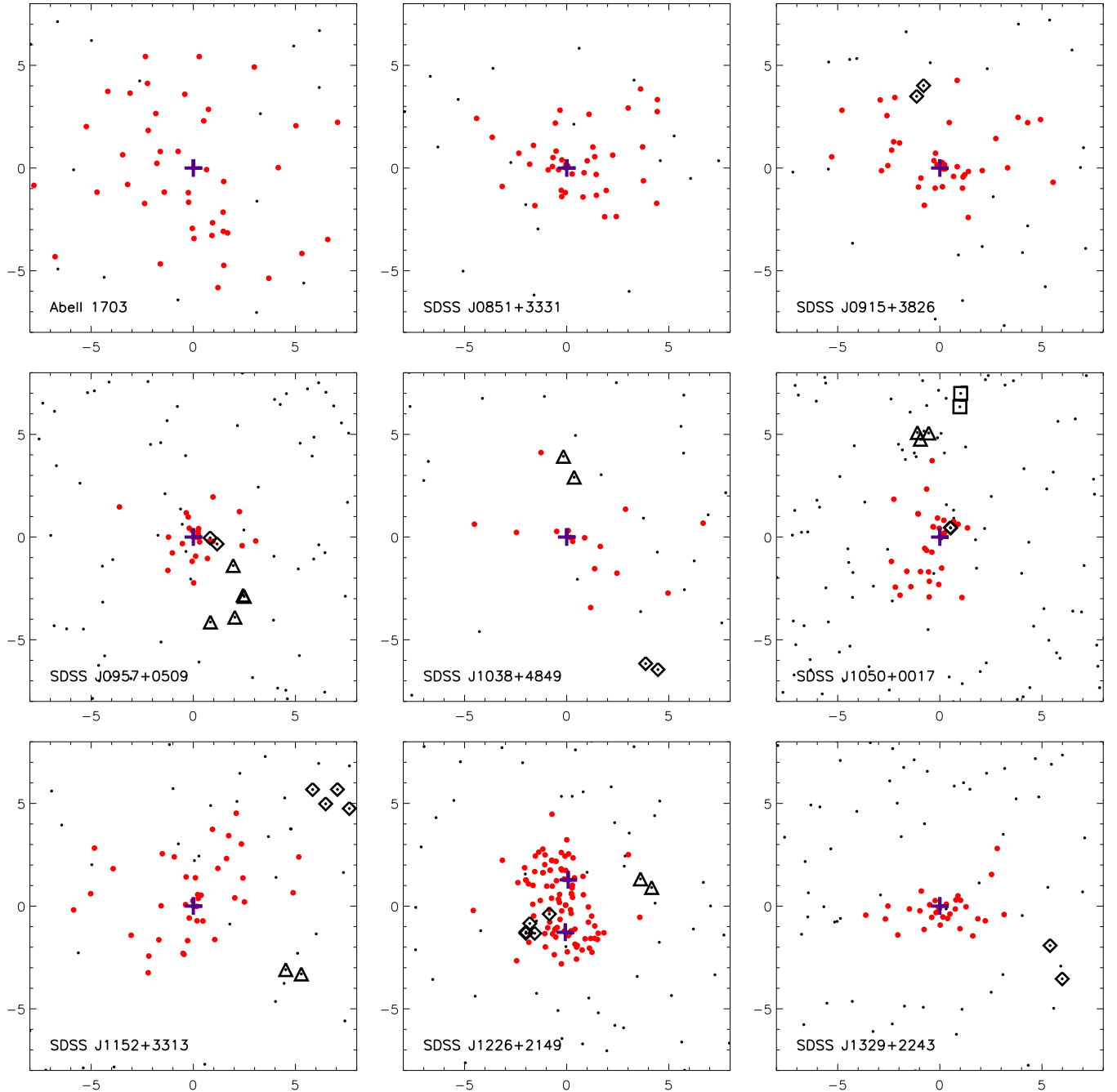


FIG. 2.— The $16' \times 16'$ region of the sky centered on each of the strong lensing cluster fields; the positions of all galaxies with spectroscopic redshifts are plotted using different symbols to indicate type. Filled larger red dots are cluster member galaxies, filled smaller black dots are field galaxies that are not associated with the cluster. Galaxies that are associated with one of the groups identified in § 3.2 are also indicated by an open black plot symbol, with different symbols corresponding to different groups identified in a given field. The centroid of the strong lensing is always indicated by a blue cross (SDSS J1226 has two cluster cores that are strong lenses, each is indicated by its own blue cross). In the line of sight centered on SDSSJ 1050+0017 there is a group located near the lensing cluster core with $N = 2$ spectroscopic members that are separated by $\sim 2''$.

Depending on how aggressively we want to define “uncorrelated” we can make several cuts on our group sample based on the comoving separation between each group and their associated primary cluster lenses. Bahcall et al. (2003) measured the correlation length to grow from ~ 16 Mpc to ~ 34 Mpc for groups and rich clusters, respectively; these numbers provide guidance for what cuts on the comoving distance we should use to pick out the structure that is uncorrelated. For all anal-

yses that follow we make two such cuts: 1) the more aggressive cut labels uncorrelated structures as only groups that are separated by a comoving distance, $D_m > 100$ Mpc from the primary cluster lenses, and 2) the less aggressive cut uses $D_m > 30$ Mpc.

In Figure 2 we plot the spectroscopic data – with all groups separated by a comoving distance of at least 30 Mpc and cluster members marked – in the regions of sky centered on each primary lensing cluster. Figure 3

TABLE 4
EXAMPLE GROUPS

α J2000	δ J2000	z	N_{gal}	σ_v^a (km s^{-1})	θ_{proj} (arcmin)
13 14 52.2	+52 03 35	0.30280	2	—	14.7
13 15 46.1	+51 51 44	0.27566	2	—	6.9
13 16 14.2	+51 40 30	0.29869	4	195	13.7
13 13 26.4	+51 49 44	0.38489	2	—	15.3
13 14 39.8	+51 59 08	0.05955	5	141	10.8
13 14 20.3	+51 41 37	0.10094	2	—	10.2
13 15 23.6	+52 02 42	0.05971	2	—	13.9

^a Computed using the gapper statistic (Beers et al. 1990) only for groups with $N_{gal} \geq 4$.

shows the distribution of group positions relative to their associated strong lensing clusters, with both the 30 Mpc and 100 Mpc cuts indicated. The final group catalog along each strong lensing selected line of sight is also summarized in Table 5.

3.3. Selection Effects In the Galaxy Redshift Catalogs

The catalog of spectroscopic redshifts that we have for each cluster is subject to important observational selection effects that we must take into account before interpreting the results of the preceding analysis. Most importantly, the multi-slit and multi-fiber spectroscopic observations that we use were designed with the primary goal of measuring cluster member redshifts in each primary lensing cluster. We used a red sequence and blue cloud selection at the lensing cluster redshift to give higher weights/priorities to the placement of slits/fibers onto likely cluster members. In practice, only a modest fraction of slits/fibers could be placed on likely members in any given slit mask or fiber configuration (due to practical considerations such as limited source density of candidate members and slit/fiber collisions).

From Table 3 we see that cluster members always make up less than 45% of our redshift sample, and typically they represent only ~ 15 -20% of redshifts in a given cluster lens field. Thus, while we recover many non-cluster member redshifts in each of our fields, our observational strategy nevertheless biases us against identifying line-of-sight structures, in favor of better sampling the primary lensing cluster velocity distributions.

We also note that the cluster members are typically spatially concentrated in the core of each primary cluster lens, so that our non-cluster member redshifts are preferentially at larger angular separations from the lensing cluster than they would have been had the slit/fiber placement had been purely random (or based purely on a simple criterion such as magnitude). This effectively biases us against identifying projected structures with small projected angular separations from the lensing clusters. This bias is additive with the one discussed above in that it hinders our ability to identify groups in our spectroscopic data. The bias against identifying line-of-sight structures near the cores of our cluster lenses is likely most evident in the lines of sight centered around Abell 1703 and SDSS J0851+3331; the spectroscopic catalog for both of these lines of sight is dominated by cluster member galaxies within a $10'$ radius of the strong lensing cluster cores, and we identify no FoF groups within these regions.

Our method of identifying candidate line-of-sight structures depends solely on the locations of galaxies in the sky and in recession velocity. It is, of course, also possible to search for group and cluster-like structures using a red sequence selection in the available imaging. However, such a selection would only find evolved/collapsed structures, while possibly missing small group-like structures that are still in the process of forming and have not yet developed a population of passively evolving member galaxies. Additionally, the purity and completeness of a red sequence selection becomes significantly worse in the smallest structures (groups with very low numbers of galaxies) (e.g., Koester et al. 2007). These smaller, lower-mass – and often less-evolved – structures are far more numerous than more massive groups and are therefore most likely to produce a chance line-of-sight alignment with a massive cluster lens. Because these chance alignments are precisely what we wish to measure, a simple red-sequence search for line-of-sight structure is not ideal for the analysis that we perform in this paper.

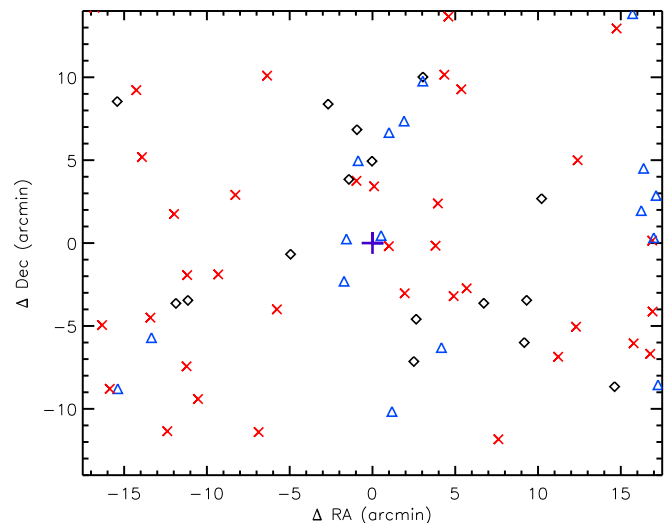


FIG. 3.— All groups identified in our spectroscopic data are plotted at their positions relative to the 10 strong lensing cluster cores analyzed in this work (SDSS J1226+2149 has two distinct strong lensing cores). The fiducial strong lensing centers are identified with the purple cross, and groups are split into two groups. Red X's indicate groups that are separated from the primary lensing clusters by > 100 Mpc along the line of sight; these are structures that we can confidently label as uncorrelated with the primary cluster lens. Blue triangles indicate groups that are separated by > 30 Mpc but less than 100 Mpc – these are also likely to be uncorrelated with the primary cluster lenses. Black diamonds indicate groups separated by ≤ 30 Mpc along the line of sight, and are therefore very possibly correlated with the primary cluster lens (we do not consider these groups in our measurement of the uncorrelated line-of-sight structure). The plot displays a $35' \times 28'$ field of view, which matches the field covered by the Subaru/SuprimeCam imaging that was used for fiber/slit placement in our spectroscopic observations.

3.4. Quantifying of Line-of-Sight Structure

We want to test the hypothesis that strong lensing clusters preferentially lie along lines of sight that have systematically more intervening structure than would be expected along random lines of sight. Quantifying the excess (or dearth) of structure along the line of sight toward our strong lensing clusters therefore must be compared against a measurement of the amount of intervening structure along random lines of sight. We previ-

ously adopted the group-finding algorithm that was used to produce the zCOSMOS 10k group catalog, making it an ideal dataset for comparing against our measurements. The zCOSMOS 10k group catalog is defined from a spectroscopic catalog that includes ~ 6500 redshifts in the interval, $0.1 < z < 0.8$, from a 1.7 deg^2 region on the sky (Knobel et al. 2009). In comparison, our data include 1707 redshifts in the same interval, covering a 2.3 deg^2 area on the sky. Our coverage is therefore $\lesssim 25\%$ as dense as the zCOSMOS 10k catalog, so that any comparison of groups identified in our data will necessarily represent a *lower limit* on the number of groups that would be identified in a dataset with spectroscopic coverage as dense as the zCOSMOS 10k catalog.

Because our spectroscopic data is more sparsely sampled than the zCOSMOS 10k catalog it is not valuable to compare the simplest observable quantities, such as a count of the number of groups that are projected within various angular separations of our strong lensing clusters. We can, however, measure the distribution of angular separations between our strong lensing clusters and the groups that we identify along each line of sight. The sparseness of our spectroscopic data should repress the total number of groups found, but it should not impact the spatial distribution of those groups. An over-abundance of structure along the line of sight toward our strong lensing cluster sample should produce a signal in the angular separations between the cluster lenses and the groups that we identified.

We measure the distribution of angular separations between strong lensing clusters and uncorrelated groups as follows. For each strong lensing cluster core we select groups that fall within a $20'$ radius of the centroid of the strong lensing (i.e., the center of the mass distribution of the primary cluster lens) and measure the radial angular separations between strong lensing core and groups for each core-group pair. The $20'$ cutoff represents the maximum radius out to which our redshift and group catalogs extend around all of our strong lenses. All of these measurements are made using the group catalogs with both $D_M > 30 \text{ Mpc}$ and $D_M > 100 \text{ Mpc}$ cuts to isolate uncorrelated groups (see § 3.2).

For comparison against our strong lensing selected cluster sample we also measure the radial separations in the same way for our redshift catalog (the input for the FoF group finder), and also for the zCOSMOS 10k group catalog where we use the most massive groups in the catalog ($\sigma_v \geq 500 \text{ km s}^{-1}$) as the centroids for measuring radial separations. In Figure 4 we plot the probability distribution functions of angular separations between each of: 1) strong lensing clusters and uncorrelated groups, 2) strong lensing clusters and all redshift data, and 3) zCOSMOS massive groups and other uncorrelated groups in the zCOSMOS catalog. Figure 4 also shows the expectation for the observed angular separation distribution along a random line of sight that is predicted from the 2-point correlation function, which has been measured for group and cluster scale structures (as mentioned previously in § 3.2; Bahcall et al. 2003). We generate this prediction by populating a cosmological volume with structures around a fiducial cluster at $z = 0.43$ (the median redshift of our cluster lens sample), where these structures are drawn by Monte Carlo from the 2 point correlation function with correlation lengths

of $r_0 = 10, 20, \text{ and } 40 \text{ Mpc}$. We then apply the same cuts ($D_m > 30 \text{ \& } 100 \text{ Mpc}$) to remove simulated structures that are nearby the fiducial cluster and then measure the resulting distribution of projected angular separations. The resulting distributions are insensitive to the choice of correlation length, as should be expected given that our choice of relatively large (i.e., conservative) comoving distance cuts. As expected, the removal of nearby (i.e., the most strongly correlated) structure produces a prediction from the 2 point correlation function that is dominated by random/uncorrelated structure.

The angular separation distributions of the full redshift catalog and the zCOSMOS groups should be similar and increase monotonically with angular separation, which simply reflects the larger area on the sky sampled at larger angular separations. If, however, strong lensing clusters lie preferentially along lines of sight that are biased toward having more intervening structure as traced by our FoF groups then we expect the distribution of groups around strong lensing clusters to differ from that of the two control samples.

From Figure 4 it is clear that we are seeing exactly this effect, in which the distributions of groups around our strong lensing clusters are significantly weighted toward small angular separations ($\theta < 6'$). This effect is apparent in the distributions using both the 30 and 100 Mpc cuts to isolate uncorrelated structure. We can quantify the significance of the effect using the KS statistic – specifically the two sided statistic as defined in Press et al. (1992). The distribution of groups around our strong lensing clusters is found to be inconsistent with the distribution of our input redshift catalog at 2.6σ (2.4σ) for the 30 (100) Mpc cut to define uncorrelated structure. This strongly supports the hypothesis that the distribution of groups around our strong lensing clusters does not simply follow the distribution of redshifts in our spectroscopic catalog. We also find that the distribution of groups around our strong lensing clusters is inconsistent with the distribution of groups around the most massive structures in the zCOSMOS 10k catalog at 2.3σ (2.2σ) for the 30 (100) Mpc cuts; this similarly supports the argument that our strong lensing selected lines of sight are strongly (i.e., $> 2\sigma$) discrepant with clusters lying along random lines of sight. We also measure the KS statistic for our observed SL group distribution and the predicted distribution from the 2 point correlation function; the KS test results indicate that the strong lensing selected cluster represent the high end of the density of uncorrelated, project structure along the line of sight at the 2.6σ (2.3σ) for the 30 (100) Mpc cuts.

Finally, we emphasize that our results are also limited by our spectroscopic sampling, which is relatively sparse in each cluster field compared to larger, dedicated spectroscopic surveys (e.g., Jones et al. 2009; Ahn et al. 2013; Parkinson et al. 2012; Newman et al. 2013; Rines et al. 2013). Even so, we detect a clear signal indicating that galaxy clusters that are selected for strong lensing preferentially lie along lines of sight that contain an over-abundance of projected structure relative to random lines of sight on the sky. Furthermore, as discussed above in § 3.3, the primary selection effect in our redshift data is the preferential targeting of photometrically-selected candidate cluster members which would only make it less likely that we iden-

TABLE 5
GROUPS IDENTIFIED IN EACH LINE OF SIGHT

Cluster Name	# Groups	< 30 (100) Mpc	> 30 (100) Mpc
Abell 1703	7	1 (3)	6 (4)
SDSS J0851+3331	3	0 (2)	3 (1)
SDSS J0915+3826	11	5 (7)	6 (4)
SDSS J0957+0509	7	0 (0)	7 (7)
SDSS J1038+4849	10	4 (5)	6 (5)
SDSS J1050+0017	17	5 (10)	12 (7)
SDSS J1152+3313	8	0 (2)	8 (6)
SDSS J1226+2149 ^a	8	2 (5)	6 (3)
SDSS J1226+2149	6	2 (2)	4 (4)

^a Two strong lensing cluster cores are separated by ~ 500 kpc and therefore occupy a single line of sight and share a spectroscopic dataset and the resulting group catalog.

tify groups with small angular projections relative to the strong lensing clusters. This effect biases our measurement low, and our measurement is therefore a lower limit on the degree to which line-of-sight structure is biased when looking toward strong lensing selected clusters are biased.

4. DISCUSSION

4.1. Frequency of Line-of-Sight Structure: Comparison Against Semi-Analytic Predictions and LRG Over-Densities

Recent studies have identified potentially powerful strong lensing lines of sight by presupposing that the cumulative effect of multiple massive structures along a single line of sight will produce large strong lensing cross sections (Wong et al. 2012; Ammons et al. 2013; Wong et al. 2013). This is a novel approach to addressing the question of how important line-of-sight structure is to generating large strong lensing cross sections and provides an interesting point of comparison. In this paper we have approached the problem from the opposite direction, beginning with a sample of strong lensing lines of sight that are selected for high magnifications (i.e., sufficient to produce a giant arc that is visible in the SDSS), and large strong lensing cross-sections as indicated by the large Einstein radii of these lenses, all of which have $\theta_E > 5''$ (with eight of the nine having $\theta_E > 9''$).

We can compare our results against the expectation based on semi-analytic modeling; Wong et al. (2012) argue that projected structures with angular separations of $\sim 100''$ are optimal for maximizing lensing cross sections, and in Wong et al. (2013) they measure structures as traced by luminous red galaxies (LRGs) within radial apertures of $210''$. Our sample of strong lensing selected clusters have an excess of projected structure within this $210''$ aperture (Figure 4), and with the excess extending out to an aperture of $\sim 6'$. Dedicated follow-up of two LRG-over-dense SDSS fields by Ammons et al. (2013) shows that each field contains a single dominant cluster-scale structure as well as one or two additional groups lined up in projection with angular separations of $\sim 2\text{--}4'$. These systems look very much like the cluster lenses in our sample that have groups in projection at small angular distances.

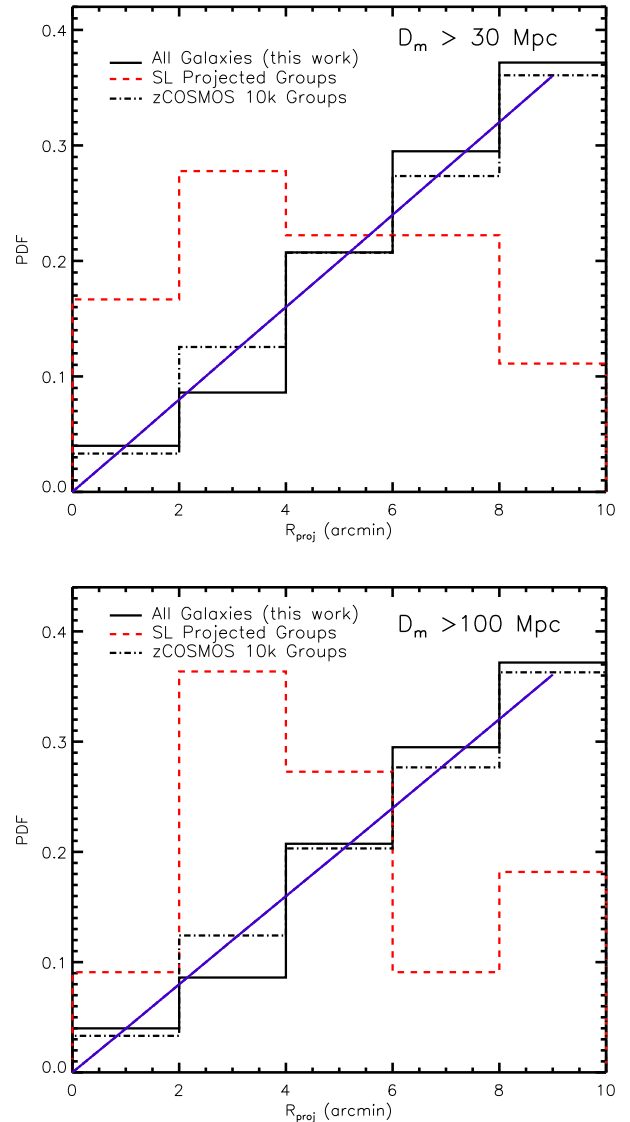


FIG. 4.— *Top*: The distribution of angular separations from the centroid of the strong lensing for both 1) all non-cluster member galaxies with spectroscopic redshifts (solid line), and 2) the groups identified in § 3.2 using the friends of friends algorithm (dashed red line). For comparison we also show the distribution of radial separations between large groups ($\sigma_v \geq 500 \text{ km s}^{-1}$) and other uncorrelated structures in the zCOSMOS 10k group catalog (dot-dashed line). The plotted distribution is the probability distribution function of angular separations from the strong lensing cluster cores (or the zCOSMOS groups with $\sigma_v \geq 500 \text{ km s}^{-1}$) extending out to a radius of $20'$. We use a comoving separation of 30 Mpc from the primary cluster lenses as the cut to define uncorrelated structure. We also plot the expected distribution of projected angular separations around a fiducial cluster along a random line of sight, as predicted by the 2 point correlation function and after also removing structures within a comoving distance of 30 Mpc (purple solid line). *Bottom*: Same as the top panel, but with a cut of 100 Mpc from the primary cluster lenses as the cut to define uncorrelated structure.

4.2. Frequency of Line-of-Sight Structure: Comparison Against Predictions from Simulations

Several studies have attempted to quantify the importance of the contribution of line-of-sight structure to the strong lensing cross sections of massive halos in cosmological simulations, drawing somewhat conflicting conclusions (Wambsganss et al. 2005; Hilbert et al. 2007;

Puchwein & Hilbert 2009). By ray tracing to recover the strong lensing cross sections of massive halos in cosmological N-body simulations, Wambsganss et al. (2005) find that $\sim 30\text{-}38\%$ of lensed sources occur because of contributions to the surface mass density from additional structures along the line of sight that are not physically associated with the primary lensing mass distribution.

Hilbert et al. (2007), on the other hand, perform a ray-tracing analysis of cluster-scale haloes in the Millennium Simulation and find that the mass attributed to line-of-sight structure toward cluster lenses contributes to the total surface mass density at only the few percent level. They conclude that mass associated with structures projected along the line of sight are modest and generally much smaller than found by Wambsganss et al. (2005). However, in a later analysis of strong lensing by clusters in the Millennium Simulation, Puchwein & Hilbert (2009) find that line-of-sight structure increases the total strong lensing optical depth by $\sim 10\text{-}25\%$, and can frequently boost the strong lensing cross sections of individual clusters by as much as 50%. This result is much more in line with the findings of Wambsganss et al. (2005), and leaves us with a rather confusing picture of what simulations have to say regarding the role of line-of-sight structure in generating strong lensing galaxy clusters.

Specific predictions from simulations regarding increases in global strong lensing optical depth by galaxy clusters are not robustly testable using observations because we have no means of confidently attributing individual instances of strong lensing to the presence of line of sight structures. However, our results are qualitatively consistent with the claims of Wambsganss et al. (2005) and Puchwein & Hilbert (2009) that line of sight structure has a significant impact on the generation of large strong lensing cross sections, and therefore on many instances of cluster-scale strong lensing.

4.3. *Implications for Strong Lensing Deep Fields and Cluster Cosmology*

Our observational results also have important implications regarding the efforts to reconstruct precision strong lens models and constrain the magnification of lensed background sources. D’Aloisio et al. (2013) find that uncorrelated structure along the line of sight can often contribute fluctuations in the magnification of background sources at the $\sim 30\%$ level for magnifications of $\sim 10\times$. Perturbations of this size are significantly larger than the typical uncertainty in the magnifications of strongly lensed sources that are estimated from high-fidelity strong lens models for cluster lenses (e.g., Kneib & Natarajan 2011; Sharon et al. 2012). We have shown here that strong lensing galaxy clusters are biased toward lying along lines of sight with a large amount of intervening structure. It is therefore crucial that current and future efforts to use galaxy cluster lenses as cosmic telescopes account for the additional uncertainty in the strong lensing models due to line-of-sight structure. Non-parametric and hybrid methods for strong lensing reconstruction (e.g., Bradač et al. 2005; Coe et al. 2008; Jullo & Kneib 2009) have the flexibility to allow for light deflection due to optically dark and/or uncorrelated line of sight structure. For cases where precision magnification maps are essential, it may be necessary to devote resources to characterizing structures along the line of sight

and using observations – such as velocity dispersion measurements of groups – to inform parameter-based models of those structures.

Our results have another important implication for efforts to constrain cosmological parameters by measuring the growth of structure as traced by the abundance of massive galaxy clusters as a function of mass and redshift (i.e., the cluster mass function). Current studies are limited by systematic uncertainties in measuring the masses of galaxy clusters (Benson et al. 2013; Reichardt et al. 2013). Weak lensing observations, in particular, are an important method for calibrating the normalization of other mass-observable relations (e.g., High et al. 2012), but weak lensing measurements are plagued by large scatter in the mass estimates of individual clusters due in part to line-of-sight effects. For clusters along random lines of sight, projected large scale structure induces an additional uncertainty that is effectively random (e.g., Hoekstra 2001). However, any reasonably large cosmological survey for galaxy clusters will contain a subset of strong lensing galaxy clusters, and those strong lensing clusters are not likely to lie along random lines of sight. Rather, the strong lensing clusters will preferentially be those clusters that lie along lines of sight with an over-abundance of intervening structure (and conversely, the non-strong lensing clusters will preferentially lie along under-abundant lines of sight). This means that the impact on weak lensing measurements due to line-of-sight structure for these strong lensing clusters will not be to inject an additional random scatter, but rather to systematically bias the weak lensing measurements high. The presence of strong lensing in a subset of a cosmological cluster catalog can therefore be used as information to inform mass observable scaling relations, and probabilistically reduce the uncertainty in mass measurements of individual clusters.

5. SUMMARY AND CONCLUSIONS

We have presented the first measurement of the frequency of projected structures along the line of sight toward a sample of strong lensing selected galaxy clusters. There is clear an excess (relative to random lines of sight) of projected line-of-sight structure within small ($\leq 6'$) angular apertures of our strong lensing selected cluster sample, and the distribution of structure around strong lensing groups is measured to be inconsistent relative to the expectation for a random line of sight at $\gtrsim 2.6\sigma$. The small sample size of our strong lensing cluster sample and group catalogs are responsible for limiting the confidence of our measurement, but in spite of these limitations we still find strong evidence for line-of-sight bias toward strong lensing clusters in comparisons against two independent control samples.

Furthermore, these results have implications for astrophysical and cosmological observations involving galaxy clusters. Current and future studies that aim to make use of galaxy clusters lenses to magnify the background universe should consider and account for structure that is projected along the line of sight toward strong lensing galaxy clusters. There are also exciting possibilities for taking advantage of strong lensing information in future cosmological analyses of galaxy cluster samples. From the presence or lack of strong lensing by individual clusters it is possible to infer what clusters are likely to have

excess cosmic structure projected along the line of sight, and that information may be used to reduce scatter in cluster mass measurements.

We thank Eric Bell for helpful discussion that improved the quality of this paper significantly. This work was supported by the National Science Foundation through Grant AST-1009012. Support was also provided by NASA through grant HST-GO-13003.01 from the Space Telescope Science Institute, which is operated by the Association of Universities for Research in Astronomy, In-

corporated, under NASA contract NAS5-26555, and by the FIRST program Subaru Measurements of Images and Redshifts (SuMIRE), World Premier International Research Center Initiative (WPI Initiative), MEXT, Japan, and Grant-in-Aid for Scientific Research from the JSPS (23740161). The data used in this work is publicly hosted with support from the Harvard-Smithsonian Center for Astrophysics (CfA) in collaboration with Harvard Library and the Institute for Quantitative Social Science, with infrastructure provided by Harvard University Information Technology Services

REFERENCES

- Ahn, C. P., Alexandroff, R., Allende Prieto, C., et al. 2013, ArXiv e-prints, arXiv:1307.7735
- Allen, S. W., Edge, A. C., Fabian, A. C., et al. 1992, MNRAS, 259, 67
- Ammons, S. M., Wong, K. C., Zabludoff, A. I., & Keeton, C. R. 2013, ArXiv e-prints, arXiv:1311.2583
- Bahcall, N. A., Dong, F., Hao, L., et al. 2003, ApJ, 599, 814
- Bartelmann, M., Huss, A., Colberg, J. M., Jenkins, A., & Pearce, F. R. 1998, A&A, 330, 1
- Bayliss, M. B. 2012, ApJ, 744, 156
- Bayliss, M. B., Gladders, M. D., Oguri, M., et al. 2011a, ApJ, 727, L26+
- Bayliss, M. B., Hennawi, J. F., Gladders, M. D., et al. 2011b, ApJS, 193, 8
- Bayliss, M. B., Rigby, J. R., Sharon, K., et al. 2013, ArXiv e-prints, arXiv:1310.6695
- Bayliss, M. B., Wuyts, E., Sharon, K., et al. 2010, ApJ, 720, 1559
- Beers, T. C., Flynn, K., & Gebhardt, K. 1990, AJ, 100, 32
- Benson, B. A., de Haan, T., Dudley, J. P., et al. 2013, ApJ, 763, 147
- Blanchard, P. K., Bayliss, M. B., McDonald, M., et al. 2013, ApJ, 772, 24
- Bradač, M., Schneider, P., Lombardi, M., & Erben, T. 2005, A&A, 437, 39
- Coe, D., Fuselier, E., Benítez, N., et al. 2008, ApJ, 681, 814
- Cooray, A. R. 1999, A&A, 341, 653
- Dahle, H., Gladders, M. D., Sharon, K., et al. 2013, ApJ, 773, 146
- Dalal, N., Hennawi, J. F., & Bode, P. 2005, ApJ, 622, 99
- D’Aloisio, A., & Natarajan, P. 2011a, MNRAS, 411, 1628
- . 2011b, MNRAS, 415, 1913
- D’Aloisio, A., Natarajan, P., & Shapiro, P. R. 2013, ArXiv e-prints, arXiv:1311.1614
- Dressler, A., Hare, T., Bigelow, B. C., & Osip, D. J. 2006, in Society of Photo-Optical Instrumentation Engineers (SPIE) Conference Series, Vol. 6269, Society of Photo-Optical Instrumentation Engineers (SPIE) Conference Series
- Estrada, J., Sefusatti, E., & Frieman, J. A. 2009, ApJ, 692, 265
- Fabricant, D., Fata, R., Roll, J., et al. 2005, PASP, 117, 1411
- Fassnacht, C. D., Koopmans, L. V. E., & Wong, K. C. 2011, MNRAS, 410, 2167
- Fassnacht, C. D., McKean, J. P., Koopmans, L. V. E., et al. 2006, ApJ, 651, 667
- Faure, C., Kneib, J.-P., Hilbert, S., et al. 2009, ApJ, 695, 1233
- Fedeli, C., Meneghetti, M., Bartelmann, M., Dolag, K., & Moscardini, L. 2006, A&A, 447, 419
- Flores, R. A., Maller, A. H., & Primack, J. R. 2000, ApJ, 535, 555
- Gladders, M. D., Hoekstra, H., Yee, H. K. C., Hall, P. B., & Barrientos, L. F. 2003, ApJ, 593, 48
- Gladders, M. D., Rigby, J. R., Sharon, K., et al. 2013, ApJ, 764, 177
- Grossman, S. A., & Narayan, R. 1988, ApJ, 324, L37
- Hamana, T., & Futamase, T. 1997, MNRAS, 286, L7
- Hennawi, J. F., Dalal, N., Bode, P., & Ostriker, J. P. 2007, ApJ, 654, 714
- High, F. W., Hoekstra, H., Leethochawalit, N., et al. 2012, ApJ, 758, 68
- Hilbert, S., Metcalf, R. B., & White, S. D. M. 2007, MNRAS, 382, 1494
- Hoekstra, H. 2001, A&A, 370, 743
- Horesh, A., Maoz, D., Hilbert, S., & Bartelmann, M. 2011, ArXiv e-prints, arXiv:1101.4653
- Jones, D. H., Read, M. A., Saunders, W., et al. 2009, MNRAS, 399, 683
- Jullo, E., & Kneib, J.-P. 2009, MNRAS, 395, 1319
- King, L., & Corless, V. 2007, MNRAS, 374, L37
- Kneib, J.-P., & Natarajan, P. 2011, A&A Rev., 19, 47
- Knobel, C., Lilly, S. J., Iovino, A., et al. 2009, ApJ, 697, 1842
- Koester, B. P., Gladders, M. D., Hennawi, J. F., et al. 2010, ApJ, 723, L73
- Koester, B. P., McKay, T. A., Annis, J., et al. 2007, ApJ, 660, 221
- Kurtz, M. J., & Mink, D. J. 1998, PASP, 110, 934
- Li, G. L., Mao, S., Jing, Y. P., et al. 2006, MNRAS, 372, L73
- Luppino, G. A., Gioia, I. M., Hammer, F., Le Fèvre, O., & Annis, J. A. 1999, A&AS, 136, 117
- Meneghetti, M., Bartelmann, M., Dahle, H., & Limousin, M. 2013, Space Sci. Rev., arXiv:1303.3363
- Meneghetti, M., Bartelmann, M., & Moscardini, L. 2003, MNRAS, 346, 67
- Meneghetti, M., Fedeli, C., Pace, F., Gottlöber, S., & Yepes, G. 2010, A&A, 519, A90
- Meneghetti, M., Fedeli, C., Zitrin, A., et al. 2011, A&A, 530, A17
- Mink, D. J., Wyatt, W. F., Caldwell, N., et al. 2007, in Astronomical Society of the Pacific Conference Series, Vol. 376, Astronomical Data Analysis Software and Systems XVI, ed. R. A. Shaw, F. Hill, & D. J. Bell, 249
- Mo, H. J., Jing, Y. P., & White, S. D. M. 1996, MNRAS, 282, 1096
- Newman, J. A., Cooper, M. C., Davis, M., et al. 2013, ApJS, 208, 5
- Noh, Y., & Cohn, J. D. 2011, MNRAS, 413, 301
- Oguri, M., Bayliss, M. B., Dahle, H., et al. 2012, MNRAS, 420, 3213
- Oguri, M., Lee, J., & Suto, Y. 2003, ApJ, 599, 7
- Oguri, M., Hennawi, J. F., Gladders, M. D., et al. 2009, ApJ, 699, 1038
- Parkinson, D., Riemer-Sørensen, S., Blake, C., et al. 2012, Phys. Rev. D, 86, 103518
- Postman, M., Coe, D., Benítez, N., et al. 2012, ApJS, 199, 25
- Press, W. H., Teukolsky, S. A., Vetterling, W. T., & Flannery, B. P. 1992, Numerical recipes in FORTRAN. The art of scientific computing
- Puchwein, E., Bartelmann, M., Dolag, K., & Meneghetti, M. 2005, A&A, 442, 405
- Puchwein, E., & Hilbert, S. 2009, MNRAS, 398, 1298
- Quintana, H., Carrasco, E. R., & Reisenegger, A. 2000, AJ, 120, 511
- Redlich, M., Bartelmann, M., Waizmann, J.-C., & Fedeli, C. 2012, A&A, 547, A66
- Reichardt, C. L., Stalder, B., Bleem, L. E., et al. 2013, ApJ, 763, 127
- Richard, J., Pei, L., Limousin, M., Jullo, E., & Kneib, J. P. 2009, A&A, 498, 37
- Rines, K., Geller, M. J., Diaferio, A., & Kurtz, M. J. 2013, ApJ, 767, 15
- Rizza, E., Morrison, G. E., Owen, F. N., et al. 2003, AJ, 126, 119
- Roza, E., Nagai, D., Keeton, C., & Kravtsov, A. 2008, ApJ, 687, 22
- Sharon, K., Gladders, M. D., Rigby, J. R., et al. 2012, ApJ, 746, 161
- Smargon, A., Mandelbaum, R., Bahcall, N., & Niederste-Ostholt, M. 2012, MNRAS, 423, 856
- Tadros, H., Efstathiou, G., & Dalton, G. 1998, MNRAS, 296, 995
- Torri, E., Meneghetti, M., Bartelmann, M., et al. 2004, MNRAS, 349, 476
- Wambsganss, J., Bode, P., & Ostriker, J. P. 2004, ApJ, 606, L93
- . 2005, ApJ, 635, L1
- Wambsganss, J., Ostriker, J. P., & Bode, P. 2008, ApJ, 676, 753
- Wong, K. C., Ammons, S. M., Keeton, C. R., & Zabludoff, A. I. 2012, ApJ, 752, 104
- Wong, K. C., Keeton, C. R., Williams, K. A., Momcheva, I. G., & Zabludoff, A. I. 2011, ApJ, 726, 84
- Wong, K. C., Zabludoff, A. I., Ammons, S. M., et al. 2013, ApJ, 769, 52
- Zaritsky, D., & Gonzalez, A. H. 2003, ApJ, 584, 691